Link to original published version: http://dx.doi.org/10.1061/(ASCE)HY.1943-7900.0001085

Citation: Guo Y (2015) Flow in Open Channel with Complex Solid Boundary. Journal of Hydraulic Engineering. Online before print. DOI http://dx.doi.org/10.1061/(ASCE)HY.1943-7900.0001085

Flow in open channel with complex solid boundary

Yakun Guo[1]

Abstract: A two-dimensional steady potential flow theory is applied to calculate the flow in open channel with complex solid boundaries. The boundary integral equations for the problem under investigation are firstly derived in an auxiliary plane by taking the Cauchy integral principal values. To overcome the difficulties of nonlinear curvilinear solid boundary character and free water surface being not known a *priori*; the boundary integral equations are transformed to the physical plane by substituting the integral variables. As such, the proposed approach has the advantages of (1) the angle of the curvilinear solid boundary as well as the location of free water surface (initially assumed) is a known function of coordinates in physical plane; and (2) the meshes can be flexibly assigned on the solid and free water surface boundaries along which the integration is performed. This avoids the difficulty of the traditional potential flow theory which seeks a function to conformally map the geometry in physical plane onto an auxiliary plane. Furthermore, rough bed friction induced energy loss is estimated using the Darcy-Weisbach equation and is solved together with the boundary integral equations using the proposed iterative method. The method has no stringent requirement for initial free water surface position, while traditional potential flow methods usually have strict requirement for the initial free surface profiles to ensure that the numerical computation is stable and convergent. Several typical open channel flows have been calculated with high accuracy and limited computational time, indicating that the proposed method has general suitability for open channel flows with complex geometry.

[1]Professor, School of Engineering, University of Bradford, BD7 1DP, UK. E-Mail: y.guo16@bradford.ac.uk

Key words: Potential flow; boundary value problem; iterative computation; free water surface flow; open channel

Introduction

Open channel flow, a gravity driven free surface flow, is a frequently encountered flow pattern in civil engineering. Such flow can be considered as inviscid and irrotational potential flow provided that the flow velocity is relatively high and there is no serious separation between flow and solid boundaries (Batchelor 2000; Hager 1985; White 1986; Montes 1998). Due to its practical engineering relevance, extensive studies have been conducted by researchers who have developed various potential flow theories and numerical methods to solve such flows in past decades. Among these methods, analytical/complex function theory was the first approach used to treat the problem (Guo *et al.* 1996; Guo 2005). Traditional analytical/complex function approach applied conformal mapping and obtained the solution of the problem as integral equations in the complex potential plane or an auxiliary plane (Birkhoff and Zarantonello 1957; Gurevich 1965). However such approach can only treat the flow with simple geometry and without the presence of gravity (Dias *et al.* 1987). For flow moving in a complex geometry (e.g. curvilinear solid boundary occurring in most open channel flows) and/or gravity being present, it is impossible to obtain the analytical solution using the complex function theory (Cheng *et al.* 1981; Yeung 1982; Guo *et al.* 1998). The difficulty in solving the gravity driven free water surface flows, as indicated by von Kármán (1940), is due to (1) the nonlinear character of curvilinear solid boundary conditions and (2) the boundary itself (free water surface) being unknown a *priori*. In traditional complex variable function theory method, the solution of the problem is expressed either in the complex plane or in an auxiliary plane. In those planes, however, not only the free water surface needs to be solved, but also the initially known solid boundaries become unknown and need to be determined as part of the solution (Wen and Wu 1987). This makes the problem more difficult to solve. As a result, the application of complex function theory to treat open channel flows with curvilinear solid boundaries is greatly limited (Diersch, *et al*., 1977). As such, various numerical methods have been developed to treat this flow pattern. The advantages and application of the numerical methods have greatly dwarfed the application of the complex variable function theory in potential flow.

Lauck (1925) could be considered as one of the pioneers dealing with the potential flow using complex variable function theory and numerical computation. He calculated the flow over an infinite high sharp crested weir using a successive numerical approximation (Lauck 1925). He found that the computation was only convergent for a certain flow discharge per unit width. Since his pioneering work, Southwell and Vaisey (1946) applied finite difference method to simulate the free overfall. Thom and Apelt (1961) demonstrated the advantage of computation in complex plane. The same approach was applied by Markland (1965) to treat the free overfall and by Cassidy (1965) to calculate the flow over spillway in which the convergent free water surface was obtained only for a certain flow discharge. Flow over sharp crested weir of finite height was simulated by Strelkoff (1964) and Strelkoff and Moayeri (1970) who obtained integral equations using potential and stream functions as variables. Similar to Cassidy, they only obtained the convergent solution for a certain flow discharge and Strelkoff and Moayeri (1970) only simulated the problem with horizontal and vertical walls. Free overfall was also simulated by Clarke (1965) and Montes (1992) who applied potential flow solutions and by Hager (1983) and Marchi (1993) who applied analytical approach. More recently, Castro-Orgaz and Hager (2013) applied potential flow theory to treat the open channel flow. The semi-inverse mapping of the Laplace equation was applied by Castro-Orgaz (2013a, b) to simulate open channel flow and free overfall.

In this study, the problem under investigation is expressed as a boundary value (the Riemann-Hilbert) problem and the general solution is obtained in an auxiliary plane. The boundary integral equations are then derived by taking the Cauchy integral principal values. Using arc (streamline) length to substitute the integral variables, the boundary integral equations in the physical plane are obtained with the integration performed only along solid and free water surface boundaries. For rough channel bed, the wall friction induced energy loss along channel bed can be estimated using the Darcy-Weisbach equation. A numerical iterative method is proposed to solve the boundary integral equations and the Darcy-Weisbach equation. As the convergence and stability of the iterative method is ensured (Wen and Wu 1987), this approach has no stringent requirement for initial free water surface profiles while the aforementioned methods usually have strict requirement for the initial free surface profiles to ensure the stability and convergence of the numerical algorithms (Montes 1992, Castro-Orgaz 2013a). As such, the difficulties of nonlinear solid boundary character and unknown free water surface (von Karman 1940) are overcome. The method has been applied to calculate several common open channel flows. Good agreement is obtained between calculation and measurements, demonstrating that the method has general practical engineering applications to a broad range of open channel flows in complex geometry.

Potential flow formulation

Considering flow over a bump in open channel where a Cartesian coordinate system (x, y) is established with x being horizontal and y being vertical (see Fig. 1a where points A and G refer to far upstream and far downstream respectively). Assume that the flow velocity is sufficiently high and there is no serious separation between flow and solid boundary, the flow under investigation can then be considered as two-dimensional irrotational and inviscid potential flow. Let φ be the potential function and ψ be the stream function, both are real values and satisfy the Laplace's equation. Define a holomorphic (or analytic) function f as following (von Kármán 1940; Batchelor 2000):

$$f(x+iy) = f(z) = \varphi(z) + i\psi(z) \tag{1}$$

where x and y = real values, $z=x+iy$, $i=\sqrt{-1}$. This analytical function will conformally map the flow field in the physical domain ((x, y) in Fig. 1a) to an infinite rectangular strip in the transformed domain ((φ, ψ), i.e. complex potential plane, see Fig. 1b). The lower and upper boundaries of the strip in the complex potential plane correspond to the solid boundary and free water surface in the physical plane, respectively. Solid boundary BCDE and free water surface KJ are streamlines. Without loss of generality, let the stream function ψ be zero along streamline BCDE and be q (q = flow discharge per unit width) along streamline KJ. Differentiating f with respect to z yields the complex conjugate of the velocity:

$$\frac{df(z)}{dz} = u_x - iu_y \tag{2}$$

where u_x, u_y = velocity components in the x, y directions respectively. Rewriting Eq.(2) as following:

$$\frac{df(z)}{dz} = u(z)e^{-i\beta(z)} \tag{3}$$

where u = flow velocity magnitude ($u = \sqrt{u_x^2 + u_y^2}$) and β = direction of flow velocity. Assume the total water head at point K of upstream free water surface be h_0. Taking x-axis as datum and setting the constant atmospheric pressure at the free water surface be zero, one obtains:

$$h_0 = y_0 + \frac{u_0^2}{2g} \tag{4}$$

where y_0=vertical coordinate of point K; u_0= flow velocity magnitude at point K; g = the acceleration due to gravity (see Fig.1a). Applying the Bernoulli equation along the free water surface (a streamline) yields:

$$u(z) = \sqrt{2g(h_0 - y)} \tag{5}$$

where y = ordinate of free water surface KJ.

Using analytical function f to define a transformation function t:

$$t = \eta + i\zeta = -e^{\frac{-\pi f}{q}} \tag{6}$$

where η and ζ=real values; π =3.14159. This transformation function t conformally maps the infinite rectangular strip in complex potential plane (f-plane) onto the upper half-plane of an auxiliary plane - t-plane (see Fig. 1c). The real axis of t-plane corresponds to the solid and water free surface boundaries of the flow domain in the physical plane (see Fig 1a) in which we assume φ =0 at point B.

Using the flow velocity magnitude and its direction, an analytic function (the dimensionless logarithmic velocity) can be defined in t-plane:

$$Fun(t) = \ln\frac{u(t)}{u_0} - i\beta(t) = \ln\frac{\sqrt{2g[h_0 - y(t)]}}{u_0} - i\beta(t) \tag{7}$$

The boundary conditions of the above analytical function *Fun(t)* on the real axis of *t*-plane can then be determined as:

$-\infty < \eta < 0$, $Im Fun(\eta) = -\alpha(\eta)$

$$0 < \eta < \infty, \quad \operatorname{Re} Fun(\eta) = \ln \frac{\sqrt{2g[h_0 - y(\eta)]}}{u_0} \tag{8}$$

where α = the bed slope of the channel (in radian), *Im* and *Re* = the imaginary and real parts of *Fun*, respectively. Equations (7)(8) define a boundary value (the Riemann-Hilbert) problem whose general solution can be written as (Muskhelishvili, 1965)

$$Fun(t) = \frac{\sqrt{t_O - t}}{\pi}\{\int_{-\infty}^{t_O} \frac{-\alpha(\eta)d\eta}{\sqrt{t_O - \eta}(\eta - t)} + \int_{t_O}^{\infty} \frac{\sqrt{2g[h_0 - y(\eta)]}d\eta}{u_0\sqrt{\eta - t_O}(\eta - t)}\} \tag{9}$$

where $t_O=0$. Let cross section KB and JE be far away from the bottom obstacle CD. Assume that no waves occur at KB; then the flow at the cross section KB can be considered as uniform (Vanden-Broeck 1997). As we are mostly interested in the flow field bounded by BCDE and KJ, the infinite integral intervals of the two integration terms on the right hand side of Eq. (9) can be shortened and replaced by finite integral intervals:

$$Fun(t) = \frac{\sqrt{-t}}{\pi}\{\int_{t_B}^{t_E} \frac{-\alpha(\eta)d\eta}{\sqrt{-\eta}(\eta - t)} + \int_{t_J}^{t_K} \frac{\sqrt{2g[h_0 - y(\eta)]}d\eta}{u_0\sqrt{\eta}(\eta - t)}\} \tag{10}$$

Eq. (10) is the general formula to calculate the flow field. In Eq.(10), if the solid boundary is comprised of straight segments (e.g. α = constants) and the gravity is ignored, then Eq. (10) can be analytically integrated. For open channel flows with curvilinear solid boundaries investigated here, the mathematical difficulty in obtaining the analytical solution is so far insurmountable (Cheng et al. 1981; Yeung 1982). This is because the analytical conformal mapping function for open channel free water surface flows from flow domain in physical plane to an infinite strip in *f*-plane (complex potential plane) or to the upper half plane of *t*-plane is unknown. Therefore, if η or φ is chosen as independent variable; $\alpha(\eta)$ or $\alpha(\varphi)$ (known in the physical plane) will be unknown functions. This will make the solution of (10) in *t*-plane or *f*-plane more difficult (von Kármán 1940). On the other hand, α is a known function of coordinates *x* and *y*, or of arc length *s* (see Fig. 2), in the physical plane. If we assume the position of free surface in advance, then *u* (Eq.(5)) is also a known function of coordinates *x* and *y*, or of arc length *s*, in physical plane. Therefore, we seek the solution of Eq. (10) in physical plane. This can be achieved via changing the integral variables in Eq. (10).

As shown in Fig.2, points B and K are taken as the origins of streamline (arc) coordinate along solid boundary BCDE and free water surface boundary KJ, respectively. Denote *s* as arc length of the streamline measured from B and K respectively along boundaries, the potential function at any point of solid and free water surface boundaries is then the function of *s*. From Eq.(7), we have

$t=\eta=-e^{-\pi\varphi/q}$ on BCDE (11a)

$t=\eta=-e^{-\pi(\varphi+iq)/q}=e^{-\pi\varphi/q}$ on KJ (11b)

Differentiating η with respect to the arc length *s* *s* along solid and free boundaries yields:

$$\frac{d\eta}{ds}=\frac{d\eta}{d\varphi}\frac{d\varphi}{ds}=-\frac{\pi\eta(s)u(s)}{q} \quad (12)$$

where $u(s)$ = the velocity magnitude along boundaries.

For most engineering practice, the pressure distribution along the solid boundary and the position of free water surface are the major concern in terms of cavitation damage studies and flooding forecasting. As such, we take the Cauchy principle value of Eq. (10) on real axis of *t*-plane.

Separating the real and imaginary parts of the principle value yields the equations for calculating the inclinations of the free water surface and the velocity magnitude along the solid boundary. In light of Eq.(12), the boundary integral solutions of Eq.(10) in physical plane can be obtained:

The velocity magnitude at a distance *s* from point *B* on the solid boundary BCDE is

$$\ln\frac{u_w(s)}{u_0} = \frac{\sqrt{-\eta_w(s)}}{q}\{-\int_{\eta_B}^{\eta_E}[\frac{\alpha(l)}{\sqrt{-\eta_w(l)}} - \frac{\alpha(s)}{\sqrt{-\eta_w(s)}}]\frac{\eta_w(l)u_w(l)}{\eta_w(l)-\eta_w(s)}dl + \int_{\eta_K}^{\eta_J}\ln\{\frac{\sqrt{2g[h_0-y_s(l)]}}{u_0}\}\frac{\eta_s(l)u_s(l)}{\sqrt{\eta_s(l)}[\eta_s(l)-\eta_w(s)]}dl\} - \frac{\alpha(s)}{\pi}\ln\frac{\eta_E-\eta_w(s)}{\eta_w(s)-\eta_B} \tag{13}$$

The inclination of free surface KJ at a distance *s* from point K is

$$\beta(s) = \frac{\sqrt{\eta_s(s)}}{q}\{-\int_{\eta_B}^{\eta_E}\frac{\alpha(l)\eta_w(l)u_w(l)}{\sqrt{-\eta_w(l)}[\eta_w(l)-\eta_s(s)]}dl + \int_{\eta_K}^{\eta_J}\{\frac{\ln\{\sqrt{2g[h_0-y_s(l)]}\}}{\ln(u_0)\sqrt{\eta_s(l)}} - \frac{\ln\{\sqrt{2g[h_0-y_s(s)]}\}}{\ln(u_0)\sqrt{\eta_s(s)}}\}\times \frac{\eta_s(l)u_s(l)}{[\eta_s(l)-\eta_s(s)]}dl\} + \frac{\ln\{\sqrt{2g[h_0-y_s(s)]}\}}{\ln(u_0)\times\pi}\ln\frac{\eta_J-\eta_s(s)}{\eta_s(s)-\eta_K}$$

(14)

where η_B, η_E, η_J, and η_K = values of η at points B, E, J and K, respectively, subscripts *w* and *s* denote solid/wall and free water surface boundaries, respectively. The integrations are performed along the solid boundary and free water surface in the direction of flow.

As aforementioned, cross section BK is uniform. Assume flow is two-dimensional, this cross section is then isopotential. Without loss of generality, let the potential function at BK be zero. The potential functions at a distance *s* from the cross section *BK* along solid boundary (BCDE) and free water surface (KJ) can then be calculated as:

$$\varphi_w(s) = \int_0^s u_w(l)dl \tag{15a}$$

$$\varphi_s(s) = \int_0^s u_s(l)dl \tag{15b}$$

With the inclination of free water surface having been determined, the location (coordinates) of free water surface KJ can be calculated by

$$x(s) = x_K + \int_0^s \cos\beta(l)dl \tag{16a}$$

$$y(s) = y_K + \int_0^s \sin\beta(l)dl \tag{16b}$$

where (x_K, y_K) = coordinates of point K.

When flow field is calculated, the pressure distribution along the channel bed can be determined by applying the Bernoulli's equation between far upstream and downstream cross section. For rough bed, the solid wall friction induced energy loss should be taken into account in order to have accurate calculation of pressure. This energy loss, which is usually ignored in potential flow methods, can be evaluated using the following iterative method. To this end, the Darcy-Weisbach equation is applied to estimate the continuous friction loss along solid boundary. Applying the modified energy equation yields the pressure distribution along the solid boundary (taking x-axis as basic datum):

$$\frac{P(s)}{\rho g} = h_0 - \frac{u^2(s)}{2g} - y(s) - h_f(s) = h_0 - \frac{u^2(s)}{2g} - y(s) - \frac{1}{8g}\int_0^s \frac{\lambda}{R_h} u^2(l)dl \tag{17}$$

where P = the pressure at the channel bed, h_0 = total energy head at cross section BK, ρ = water density, $h_f(s)$ = continuous energy loss generated by wall friction along the channel bed, R_h = hydraulic radius (taken as water depth); $\lambda = 8g\ n^2 / R_h^{1/3}$ = the Darcy-Weisbach coefficient (in metric units); n = the Manning coefficient, which is taken as 0.014 for concrete (Sivakumaran et al. 1983).

The boundary integral equations (13) and (14) together with Eqs. (16) and (17) form the basic equations used to calculate the flow field, pressure distribution on the bed and the position of free water surface in open channel flow. The boundary integral equations and the pressure equation will be solved using iterative method proposed below.

Boundary conditions

Boundary conditions are summarized as following: at lower solid boundary, the stream function ψ is set as zero and the geometries are prescribed, namely α is known. At upper free water surface boundary, the stream function ψ is set as q (flow discharge per unit width) and the constant atmospheric pressure is assumed to be zero. At far upstream section BK and downstream section EJ where the effect of bottom topography is assumed to be negligible, the flow is assumed to be parallel to the channel bottom (Montes 1994; Castro-Orgaz 2013a).

Computational procedure

A numerical iterative method is proposed to solve the boundary integral equations and pressure distribution equation. The computational procedure is as following:

1. Specify the inlet boundary conditions (e.g. water depth and flow velocity) according to the experiments. Assume the energy loss due to friction be zero.
2. Assume free surface KJ. Assign non-uniform meshes along boundaries with finer meshes in the regions of rapid change of flow (e.g. near the bottom obstacle). Meshes are

assigned between points *B* and *E* along solid boundary and between points *K* and *J* along free water surface. Figure 3 is an illustrative sketch to demonstrate the strategy of assigning non-uniform meshes along boundaries.

3. Assume velocity along solid boundary BCDE and calculate velocity on free water surface KJ using the Bernoulli equation.
4. Calculate potential functions using (15a, b) and η using (11a, b) on boundaries KJ and BCDE.
5. Bring these values into Eqs. (13)(14) to calculate new velocity along solid boundary BCDE and new inclination of free water surface KJ.
6. Calculate the new position of free water surface KJ using (16a, b), then calculate new velocity on free surface KJ using the Bernoulli equation (5).
7. Calculate new potential functions and η on boundaries KJ and BCDE. Estimate new friction induced energy loss.
8. Repeat steps 5 to 7 until

$$\frac{\varphi^n - \varphi^{n-1}}{\varphi^n} < \varepsilon_1; \quad \frac{h_f{}^n - h_f{}^{n-1}}{h_f{}^n} < \varepsilon_2 \tag{18a, b}$$

where superscript *n* denotes the iterative number; ε_1,ε_2 = prescribed computational accuracy for potential function and energy loss, respectively; the values of potential function and energy loss are taken at point E.

9. Calculate the pressure distribution using Eq. (17).

Numerical examples

Several frequently encountered open channel flows with various boundary conditions are simulated using the proposed method. Simulated results are well compared with measurements, demonstrating that the approach has general suitability to broad open channel flows with satisfactory accuracy.

Open channel flow over irregularities

Cavitations often occur when high speed water flows around objects, resulting in the damage of the object surface and reducing mechanical efficiency. Typical example is the cavitation caused by high velocity flow over the surface irregularities (Ball 1976). Cavitation damage takes place when the absolute pressure is equal to or lower than the vapor pressure of water at the given temperature (Douglas et al. 2001). Therefore, the most potential place that cavitation may appear is the place where the minimum pressure occurs and this can be represented using the pressure coefficient (Guo et al. 2007).

Therefore, to investigate the likelihood of cavitations around the irregularity, applying modified energy equation along the irregularity surface (which is a streamline) yields the pressure coefficient on the irregularity (taking the x-axis as datum):

$$C_p(s) = \frac{P(s) - P_0}{\rho u_0^{\ 2}/2} = 1 - \frac{u(s)^2}{u_0^{\ 2}} + \frac{2g\{h_f(s) - y(s)\}}{u_0^{\ 2}} \tag{19}$$

where C_p=pressure coefficient on the irregularity surface, P_0 = the pressure at far undisturbed upstream, $y(s)$=the height of irregularity, other symbols have the same meanings as those in Eq.(17). In general, the last item on the right hand side of Eq. (19) is much smaller than other items for relatively small irregularity and can be ignored. Equation (19) shows that the minimum pressure, thus the minimum pressure coefficient, appears at the point that the maximum velocity takes place. This is the position that the most likelihood of cavitations damage takes place.

Two types of irregularity are simulated in this study: one is arc irregularity and another is semi-arc step. Both the arc irregularity and semi-arc step were placed at the centre of the channel. The front and end edges of arc irregularity were at the same level of the channel bed (see the sketch inside Fig. 4). For semi-arc step, the channel bed at the end of semi-arc step was raised to the same level of the end edge of the step (see the sketch inside Fig. 5). Therefore, there was no abrupt drop at the back of the semi-arc step.

Fig. 4 is the plot of the simulated and measured (taken from Lin and Xu 1985) pressure coefficient distribution around arc irregularity for upstream incoming flow velocity of u_0=4.52m/s, h=0.1m (corresponding to the incoming flow Froude number $F=u_0/(gh)^{1/2}$=4.56). The height of arc irregularity is δ=0.0092m and radius R=0.6m. Simulations were performed at 10 water depths in both upstream and downstream where the effect of arc irregularity was expected to be negligible. The maximum mesh size is 0.005m at both the far upstream and downstream and the minimum mesh size is 0.0015m around the arc irregularity and the free surface above it. The simulation was performed at a Dell OPTIPLEX390. For the computational accuracy of 10^{-4} and 10^{-3} for potential function and energy loss respectively, the total computational time for all cases is less than 1 minute with iteration number being between 15 and 30.

Fig.4 demonstrates that an almost symmetric pressure coefficient distribution around the centre of the arc irregularity exists. It is seen that the pressure coefficient decreases along the irregularity and reaches the minimum value roughly at the top of irregularity. This is the location that the largest effect of the obstruction of irregularity to flow takes place, thereby producing the maximum flow velocity. This position is the location where the likelihood of cavitations may take place. Good agreement between the simulated and measured pressure coefficients indicates that the proposed method can accurately predict the flow and pressure field for flow over an irregularity in open channel.

If irregularity is sufficiently high, flow regime will be similar to that of flow over a hump (discussed below) or weir flow where flow regime changes from upstream subcritical to downstream supercritical.

Fig. 5 is the comparison of simulated and measured pressure coefficient around a semi-arc step for incoming flow velocity u_0=2.95m/s, water depth h=0.1m, irregularity height δ=0.0111m and radius R=0.6m. The corresponding incoming flow Froude number is F=2.98. The mesh assignment is similar to that in arc-irregularity. Both the measured (symbols, taken from Lin and Xu 1985) and simulated (solid lines) results show that the pressure coefficient decreases along the semi-arc step and reaches the minimum at $s/L\approx 0.82$ where the maximum velocity occurs due to the contraction effect of the step. The pressure coefficient then increases downstream.

Simulations have also been run to investigate the effect of incoming flow velocity (thus the Froude number) on the flow and pressure field. For the sake of clarity and for the purpose of comparison, measured results of u_0=6.40m/s (F=6.47) are plotted in Fig. 5, while the solid line represents the averaged simulated results for F=2.98 and 6.47. It is seen that the incoming flow velocity (or the Froude number at the inlet) has insignificant effect on the pressure distribution around the semi-arc step. Simulations run for a range of the Froude number reveals similar results.

Fig. 5 also demonstrates that relatively large deviation between the simulation and experiments exists around the top of the semi-arc step. This may be ascribed to the fact that the asymmetric step irregularity has relatively larger effect on the flow near the top step region.

Comparing Fig. 4 and Fig. 5 demonstrates that for the similar size (height and radius), arc irregularity has slightly greater impact on the flow and pressure field around irregularity than that semi-arc step irregularity does. There may be two reasons. The first reason is that the arc irregularity is almost twice long of the semi-arc step irregularity; therefore, it has larger effect on the flow than semi arc step does. The second reason is that the end of the semi-arc step is at the same level as that of the channel bed. Therefore, it is unlikely that the flow separation will take place at the end of step, which greatly reduces the impact of semi-arc step on the flow field. For cases that there exists an abrupt enlarge cross section (e.g. the end of the semi-arc irregularity is higher than the channel bed), flow separation and vortices may take place, thereby resulting in larger impact on pressure distribution around the end of irregularity. In this situation, the proposed potential flow approach fails and advanced turbulent models are required to capture the vortex flow structures at the end corner of semi-arc irregularity.

Open channel flow over a bottom hump

The second example is the open channel flow over a relatively large hump. The case simulated is taken from Sivakumaran et al. (1983) who measured the free water surface profile and bottom pressure distribution around the symmetrical and asymmetrical humps. For symmetrical hump which is expressed as $y=0.2exp[-0.5(x/24)^2]$ (in m), the unit width flow discharge is q=0.112 m^2/s (high flow) and 0.036 m^2/s (low flow), respectively. The corresponding upstream Froude number is 0.18 and 0.08, indicating that the incoming flow is subcritical for both cases. The length of the open channel simulated is about 6m with the hump located approximately centrally. In the regions where flow varies rapidly (e.g. around the hump and the free water surface above it); meshes are locally refined to improve the computational accuracy with the minimum mesh size of 0.0012m. The computational time (run on a Dell OPTIPLEX390) for all cases is less than 2 minutes for the computational accuracy of 10^{-4} for potential function.

Figs. 6(a) and (b) plot the measured (symbols) and simulated (solid and dashed lines) free water surface and bottom pressure distribution around the hump. Fig. 6 shows that water flow accelerates as it approaches the hump. The flow continues accelerating and descends down the lee side of the hump. The simulation shows that the flow transition from subcritical to supercritical roughly takes place at the crest of hump for both cases. In contrast to free water surface, the bed pressure decreases as flow approaches the hump and reaches the minimum in the half top lee side of hump. This is caused by the variation of water depth as well as the profile of hump. The water depth at the half top lee side is relatively small while the hump convex profile produces the negative centrifugal force, resulting in the minimum pressure. The bed pressure then slightly increases downstream due to the contribution of centrifugal force generated by the concave profile of the hump. The good agreement between the simulated and measured free water surface and bed pressure for both cases indicates that the proposed potential flow method performs well for both subcritical and supercritical flow.

Flow over asymmetrical hump is also simulated. In this case, the hump is a B-splined shape (Sivakumaran et al. 1983). The flow discharge per unit width is q=0.11165 m^2/s. The corresponding upstream Froude number is 0.12, indicating that the upstream incoming flow is subcritical. The mesh assignment is similar to that for symmetrical hump. The simulated and measured free water surface and bed pressure distribution are plotted in Fig. 6c. The simulation shows that the flow transition from subcritical to supercritical takes place roughly at the hump crest, while this flow transition takes place slightly downstream of the hump crest in the experiments. It is also seen that the potential flow method underestimate the bed pressure. Runs using finer meshes (the minimum meshes around asymmetrical hump is 0.0008m) didn’t improve the computational accuracy. This discrepancy between simulation and measurement may be ascribed to the fact that the asymmetrical hump shape has larger impact on flow field with larger extensive flow transition region (Sivakumaran et al. 1983); which the potential flow approach may fail to accurately capture.

Flow transition in curved open channel

Flow in an open channel with the bed slope changing from mild to steep (or other way round) is frequently encountered in men-made flows. Free overfall usually takes place at the slope break. The water depth upstream the slope break is larger than the critical water depth, while the water depth downstream the slope break is smaller than the critical water depth. The determination of the free water surface is of importance due to its practical engineering applications (Chow 1959; Montes 1994). As flow regime changes from subcritical in the upstream mild slope section to supercritical in the downstream steep slope reach, free water surface goes through a sharp drop which provides a challenge for accurate simulation. In this study, the flow transition from mild slope to steep slope is simulated using the proposed potential flow method. The simulation case is taken from Montes (1994). Though details can be found in Montes (1994), we present a brief description here for convenience. The upstream horizontal plane was connected with a steep slope of either 45^0 or 60^0 via a circular fairing of radius r=0.1m. The flume width was 0.402m. The flow discharge simulated for both cases is 0.06m^3/s. The data of free water surface profiles and bed pressure are taken from Montes (1994) for the purpose of comparison with the simulation.

For the given experimental data, the flow at upstream horizontal section is critical and transfers to supercritical as it moves towards the steep slope. Simulation was performed 10 upstream water depths in both upstream and downstream reaches. The maximum mesh size is 0.008m at both the far upstream and downstream and the minimum mesh size is 0.004m around the circular fairing section and the free water surface above it. The simulated and measured free water surfaces and bed pressure distributions are plotted in Fig. 7 for a steep slope of 45^0 (Fig. 7a) and 60^0 (Fig. 7b) in which h is water depth at upstream mild slope section. The simulated end depth ratio (depth at the end of mild slope to critical depth) is 0.703 for 45^0 and 0.692 for 60^0 respectively. These values are slightly smaller than the classic result of Rouse (1936) for a horizontal channel and favorably compare with the experiments taken from Montes (1994). For both cases, the simulation shows that water depth continues to decrease over the short circular transition section and steep slope. In general, good agreement between the simulated and measured free water surface profiles is obtained.

It is seen from Fig. 7 that both the simulations and experiments demonstrate that the bed pressure sharply decreases at the circular section. This can be ascribed to the centrifugal force caused by convex curve solid boundary as well as the decrease of water depth. The minimum bed pressure appears at the lower part of the circular linkage for two steep slopes. The bed pressure then increases and reaches the positive value near the beginning section of the steep slope where the centrifugal force disappears. Comparison of simulation and measurements demonstrates that the proposed potential flow method favorably predicts the sharp variation of the bed pressure distribution around the transition from mild to steep slopes. Fig. 7 also shows that the simulation slightly overestimates the minimum bed pressure.

Simulations have also been performed for various flow discharges. Similar results to Fig. 7 are obtained. Simulation reveals that the absolute value of the minimum bed pressure decreases with the decrease of flow discharge.

Flow through spillway flip bucket

Spillway is usually used to discharge water from a reservoir into downstream with a free jet. The flow characteristics (e.g. free water surface profiles, bottom pressure, etc) in the spillway flip bucket are of importance to optimize the design of the spillway. The profile of flip bucket has significant effect on the free trajectory jet exiting from the bucket. In this study, a circular flip bucket with different Froude numbers is simulated and compared with the measurements taken from Lenau and Cassidy (1969). The central angle of bucket (or total turning angle of bucket) simulated is 95^0 and the slope angle of upstream spillway chute is 56.16^0 (see the inset sketch in Fig.8). Simulation was performed from 10 upstream water depths from the entrance of the flip bucket. Meshes are locally refined within the bucket to ensure the computational accuracy. Two upstream incoming flow Froude numbers F=7.35 and 10.39 are simulated, corresponding to the ratios of bucket radius to the depth of flow well upstream from bucket being 3 and 6 respectively. Figure 8 shows the comparison of simulated and measured (taken from Lenau and Cassidy 1969) bucket bottom dimensionless pressure distribution for (a) F=7.35 and (b) 10.39. In Figure 8, s is the arc distance from the starting point of flip bucket and L is the total arc length of bucket. It is seen that bottom pressure increases sharply as flow enters into bucket. This is mainly caused by the centrifugal force due to the concave curve solid boundary. The bottom pressure then remains approximately constant in the bucket. The bottom pressure then sharply decreases as flow approaches exit and becomes zero at the exit. Comparing Fig 8a and 8b demonstrates the bottom pressure in the bucket decreases with the increase of the incoming Froude number. In general, simulated bottom pressure agrees well with the measurements though a slight discrepancy between simulation and measurement takes place at the entrance of bucket.

Conclusion

Open channel flow over curved boundary or irregularities/humps is frequently encountered in civil engineering. Potential flow theory has been applied to calculate such flows due to its simple form and easy calculations (Castro-Orgaz 2013a). However, traditional complex variable function approach can only treat flow in simple geometry comprised by straight sections and without the presence of gravity. For free water surface open channel flows with curvilinear solid boundaries, the mathematical difficulty is so far insurmountable (Cheng et al. 1981; Yeung 1982) due to the fact that the boundary condition is nonlinear and the free water surface is unknown a *priori* (von Kármán 1940). In this study, the boundary integral equations for the problem under investigation are derived in an auxiliary plane by taking the Cauchy integral principal values. Using the arc length to substitute the integral variables yields the boundary integral equations in the physical plane. The advantage of expressing boundary integral equations in the physical plane is that both the angle of the prescribed curved solid boundary and position of free water surface (assumed in advance) are known functions of coordinates x and y, or of arc length s, in physical plane. The effect of rough boundary friction is evaluated using the Darcy-Weisbach equation. An iterative computational method is proposed to solve the boundary integral equations and the Darcy-Weisbach equation. As the integration is performed only along the solid and free water surface boundaries, the computational meshes can be flexibly assigned along boundaries to ensure simulation accuracy and save computational time. When flow discharge is known, the convergence and stability of the numerical iteration has been proved (Wen and Wu 1987). Therefore, the proposed method has no stringent requirement for initial values and position of free water surface while other potential flow methods usually have high requirement for the initial free water surface profiles in order to have a convergent numerical solution (Montes 1992, Castro-Orgaz 2013a). The approach has been successfully applied to calculate several common open channel flows in various boundary conditions for a range of flow parameters. The position of free water surface and pressure distribution at the channel bed can be accurately simulated using the proposed method. Examples carried out in this study demonstrate that the proposed approach can provide quick and accurate solution to frequently encountered engineering problems. Given that for most engineering practice, the location of free water surface, bottom pressure distribution and flow rate are the most concerned aspects in terms of flooding forecasting and prediction and cavitation damage studies; the proposed approach has the broad engineering practice applications.

For cases that only water depth upstream is given, the iterative approach based on consistency between the discharge and uniform velocity at far upstream can be used to determine flow discharge (Guo et al. 1996, 1998). The iterative method for flow discharge will then be incorporated into the iterative procedure for computing free water surface and bottom pressure to form a synchronous iteration (Guo et al. 1996, 1998).

If serious flow separation between flow and solid boundary takes place or if the turbulent properties are of importance for the problem under investigation, the proposed potential flow approach cannot capture these details of flow structures. For these flow scenarios, the more sophisticated and complex turbulent models should be used.

Acknowledgement: The writer is grateful for the financial support of this study by the Open Fund from the State Key Laboratory of Hydraulics and Mountain River Engineering, Sichuan University (SKHL1302). The comments and suggestions made by the Associate Editor and three Reviewers have greatly improved the quality of the final manuscript.

Notation

The following symbols are used in this paper:

C_p=pressure coefficient;

F=the Froude number;

$f=\varphi+i\psi$;

Fun=analytical function or dimensionless logarithmic velocity;

g=acceleration due to gravity;

h=water depth at cross section BK;

h_0= total water head upstream;

h_f= continuous energy loss due to friction;

$i=\sqrt{-1}$

L=total arc length of arc, semi-arc irregularity or flip bucket;

n= the Manning's roughness;

P = the pressure at the channel bottom

P_0 = the pressure at far undisturbed upstream;

R=radius of arc and semi-arc irregularity;

R_h = hydraulic radius;

r= radius of a circular fairing connecting mild and steep slopes;

s=arc length from the starting point of irregularity or flip bucket;

u=flow velocity magnitude;

u_x, u_y= velocity components in the x, y directions, respectively

u_0 = the velocity at far upstream;

α= the bed slope of the channel;

β= direction of flow velocity;

λ = the Darcy-Weisbach coefficient

π= 3.14159;

φ= potential function;

ψ= stream function;

ε_1= prescribed computational accuracy for potential function;

ε_2= prescribed computational accuracy for energy loss;

References

Ball, J.W. (1976). "Cavitation from surface irregularities in high-velocity." *J. Hydraul. Div.* 102(9), 1283-1297.

Batchelor, G.K. (2000). *An introduction to fluid dynamics*, Cambridge University Press. Cambridge, New York.

Birkhoff, G. and Zarantonello, E.H. (1957). *Jets, wakes and cavities*. Academic Press, New York.

Cassidy, J.J., (1965). "Irrotational flow over spillways of finite height." *J. Eng. Mech. Div.* 91(6), 155-173.

Castro-Orgaz, O. (2013a). "Potential flow solution for open channel flows and weir-crest overflow." *J. Irrigation and Drainage Engineering,* 139(7), 551-559.

Castro-Orgaz, O. (2013b). "Iterative solution for ideal fluid jets." *J. Hydraul. Eng.*, 139(8), 905-910.

Castro-Orgaz, O. and Hager, W.H. (2013). "Velocity profile approximation for two-dimensional potential open channel flow." *J. Hydraul. Rese.* 51(6), 645-655.

Cheng, A.H-D., Liggett, J.A., and Liu, P.L-F. (1981). "Boundary calculations of sluice and spillway flow." *J. Hydr. Div.*, ASCE, 107(10), 1163-1178.

Chow, V.T. (1959). *Open-Channel Hydraulics.* McGraw-Hill book Company, New York.

Clarke, N.S. (1965). "On the two-dimensional inviscid flow in a waterfall." *J. Fluid Mech.*, 22(part II), 359-369.

Dias, F., Elcrat, A.R. and Trefethen, L.N. (1987). "Ideal jet flow in two dimensions." *J. Fluid. Mech.,* 185, 275-288.

Diersch, H.J., Schirmer, A., and Busch, K.F. (1977). "Analysis of flows with initially unknown discharge." *J. Hydr. Div.*, ASCE, 103(3), 213-232.

Douglas, J.F., Gasiorek, J.M., and Swaffield, J.A., (2001). *Fluid Mechanics*, 4th Edition, Pearson & Prentice Hall, London, New York.

Guo, Y.K., (2005). “Numerical modelling of free overfall.” *J. Hydraul. Eng.*, 131(2), 134-138.

Guo, Y.K., Wen, X., and Wu, C.G. (1996). "Flow through slit in dam." *J. Hydraul. Eng.*, 122(11), 662-669.

Guo, Y.K., Wen, X., Wu, C.G., and Fang, D. (1998). “Numerical modelling of spillway flow with free drop and initially unknown discharge.” *J. Hydraul. Res.*, 36(5), 785-801.

Guo, Y.K., Wang, P.Y., and Zhou, H.J. (2007). “Modelling study of the flow past irregularities in a pressure conduit.” *J. Hydraul. Eng.*, 133(6), 698-702.

Gurevich, M.I. (1965). *Theory of jets in ideal fluids*. Academic Press, New Youk.

Hager, W.H. (1983). "Hydraulics of plane free overfall." *J. Hydraul. Eng.*, 109(12), 1683-1697.

Hager, W.H. (1985). “Critical flow condition in open channel hydraulics.” *Acta Mech.*, 54, 157-179.

von Kármán, T. (1940). “The engineer grapples with nonlinear problems.” *Bull. Amer. Math. Soc.* 46(8), 615-683.

Khan, A.A., and Steffler, P.M. (1996). "Modeling overfalls using vertically averaged and momentum equations." *J. Hydraul. Eng.*, 122(7), 397-402.

Lauck, A. (1925). “Der überfall über ein wehr.” *Zeitschrift für Angewandte Mathematik und Mechanik.* 5, 1-16.

Lenau, C.W. and Cassidy, J.J. (1969). “Flow through spillway flip bucket.” *J. Hydr. Div.*, ASCE, 95(HY2), 663-648.

Lin, B.Y. and Xu, X.Q. (1985). “Analysis of two-dimensional cavity flow by finite element.” *Applied Mathematics and Mechanics*,6(5), 465-474.

Marchi, E. (1993). "On the free overfall." *J. Hydraul. Res.,* 31(6), 777-790.

Markland, E. (1965). “Calculation of flow at a free overfall by relaxation method.” *Proc. Proc. Inst. of Civ. Engrs.,* 31, Paper 686, 71-78.

Montes, J.S., (1998). *Hydraulics of open channel flow.* ASCE Press, Reston, VA.

Montes, J.S. (1992). "A potential flow solution for the free overfall." *Proc. Inst. of Civ. Engrs., Water, Maritime and Energy,* Vol. 96, 259-266.

Montes, J.S. (1994). “Potential-flow solution to 2D transition from mild to steep slope.” *J. Hydraul. Eng.*, 120(5), 601-621.

Muskhelishvili,N.I., (1966). *Singular Integral Equations* (in Chinese, translated from Russian). Shanghai Science and Technology Press.

Rouse, H. (1936). "Discharge characteristics of the free overfall." *Civ. Engrg.*, 6(4), 257-260.

Sivakumaran, N.S., Tingsanchali, T. and Hosking, R.J. (1983). “Steady shallow flow over curved beds.” *J. Fluid Mech.* 128, 469-487.

Southwell, R., and Vaisey, G. (1946). "Relaxation methods applied to engineering problems. XII. Fluid motions characterized by 'free' streamline." *Philosophical Trans. Royal Soc.*, Series A, London, England, 240, 117-161.

Strelkoff, T.S. (1964). “Solution of highly curvilinear gravity flows.” *J. Energ. Mech. Div.*, 90(3), 195-221.

Strelkoff, T.S., and Moayeri, M.S. (1970). “Pattern of potential flow in a free overfall.” *J. Hydraul. Div.*, 96(4), 879-901.

Thom, A. and Apelt, C. (1961). *Field computations in engineering and physics,* Van Nostrand, London.

Vanden-Broeck, J.-M., (1997). "Numerical calculation of the free-surface flow under a sluice gate." *J. of Fluid Mech.,* 330, 339-347.

Wen, X.Y. and Wu, C.G. (1987). "Boundary integral equation – inverse method for free surface gravity flows." *Scientia Sinica*, *Series A,* 30(9), 992-1008.

White, F.M., (1986). *Fluid Mechanics*, 2nd Edition, McGraw-Hill Book Company.

Yeung, R.W., (1982). "Numerical methods in free-surface flows." *Ann. Rev. Fluid. Mech.,* 14, 395-442.

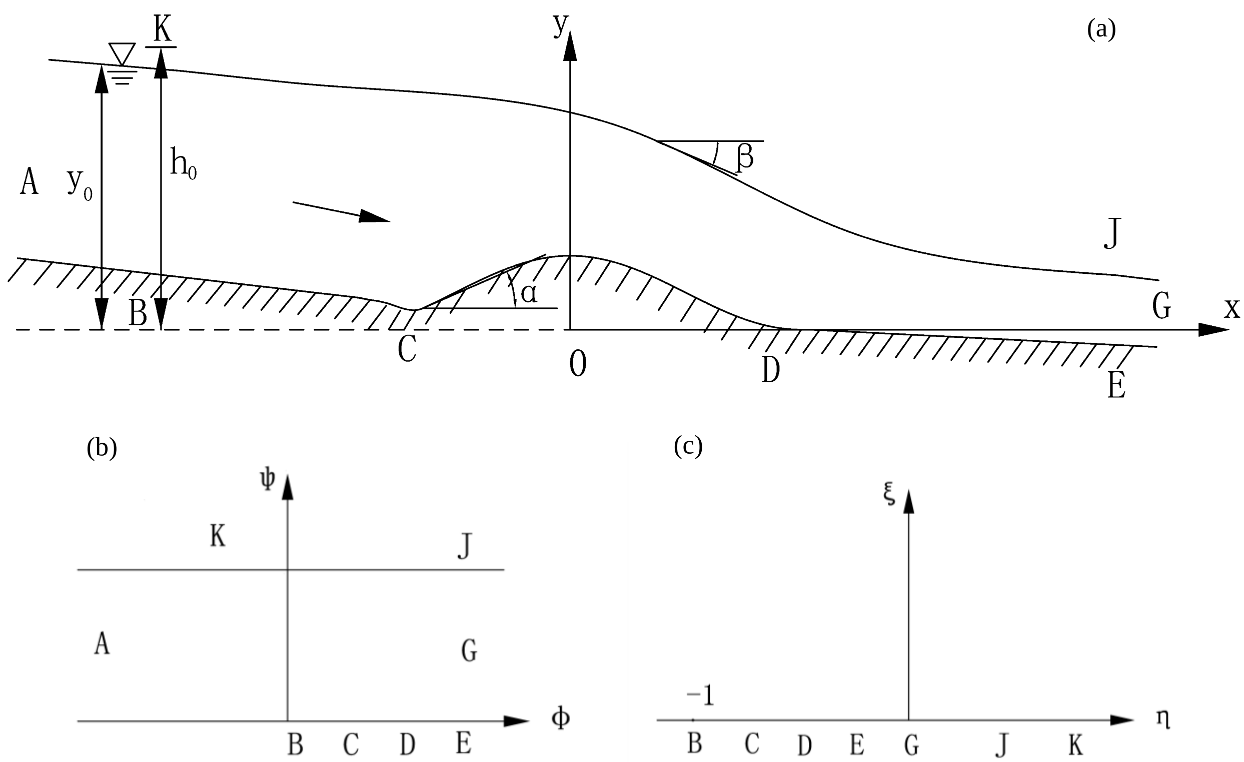

Figure 1. Schematic diagram of open channel flow over a bottom obstacle; (a) flow domain in physical plane; (b) in complex potential plane ((φ, ψ) plane) and (c) in an auxiliary plane - t-plane.

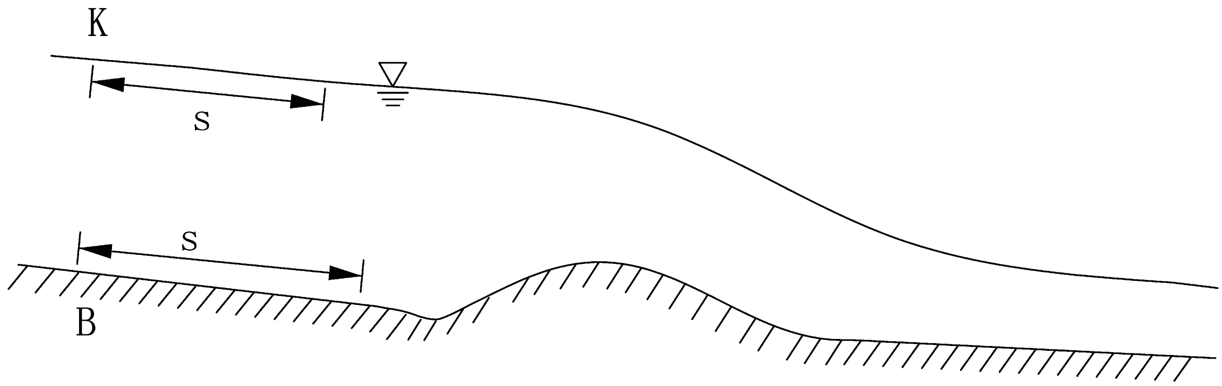

Figure 2. Sketch of streamline coordinate system.

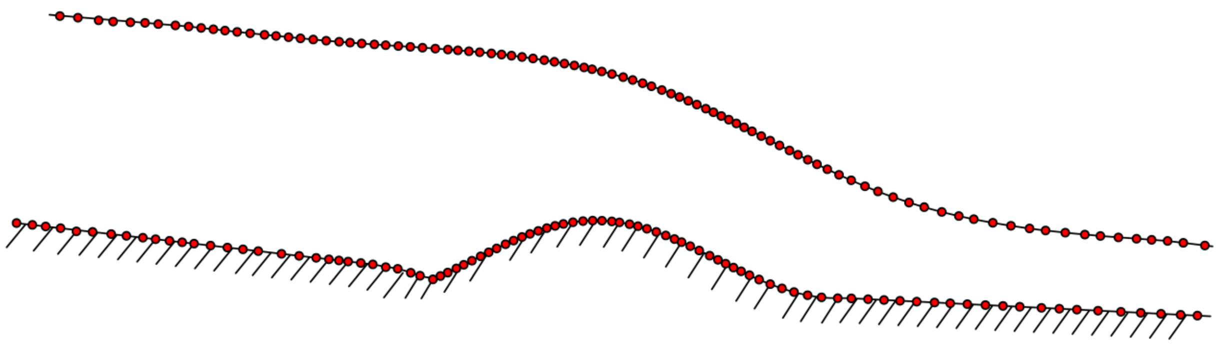

Figure 3. Sketch of meshes along solid and free water surface boundaries for demonstrating the strategy of meshes assignments.

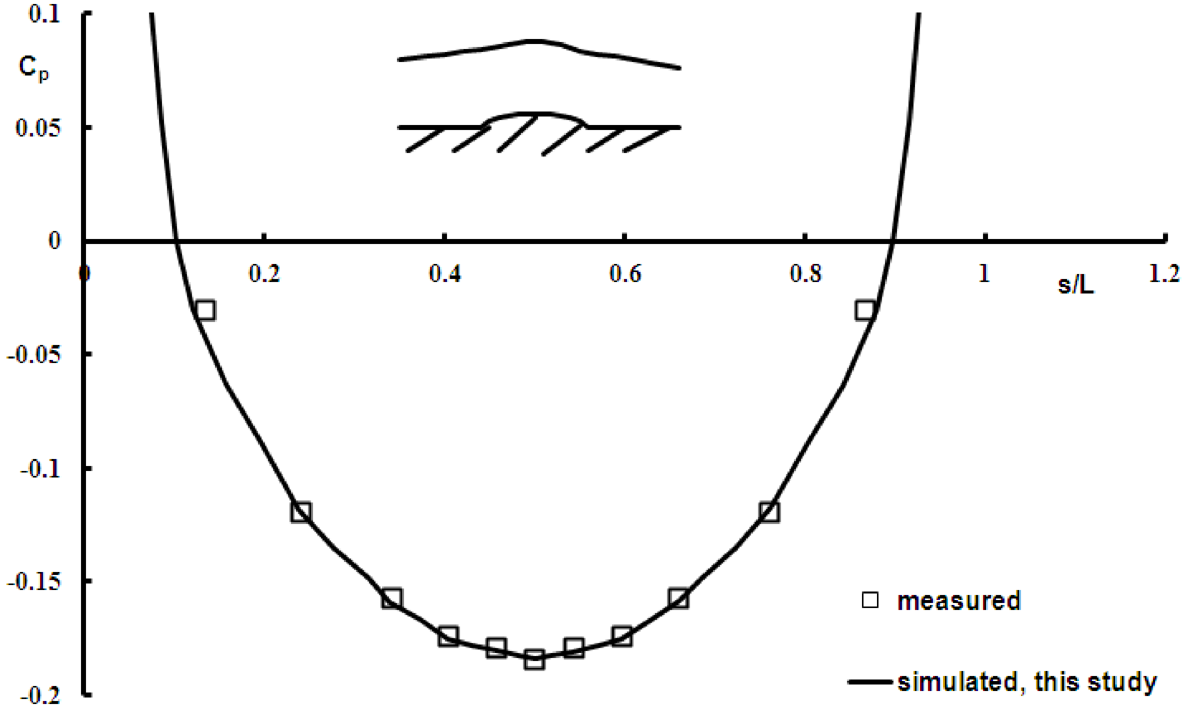

Figure 4. Comparison of the simulated (solid line) and measured (symbol) pressure coefficient distribution around the arc irregularity, *s* is the streamline distance from the starting point of the arc irregularity and *L* is the total streamline length of the arc irregularity. Inset is the sketch of experimental set-up.

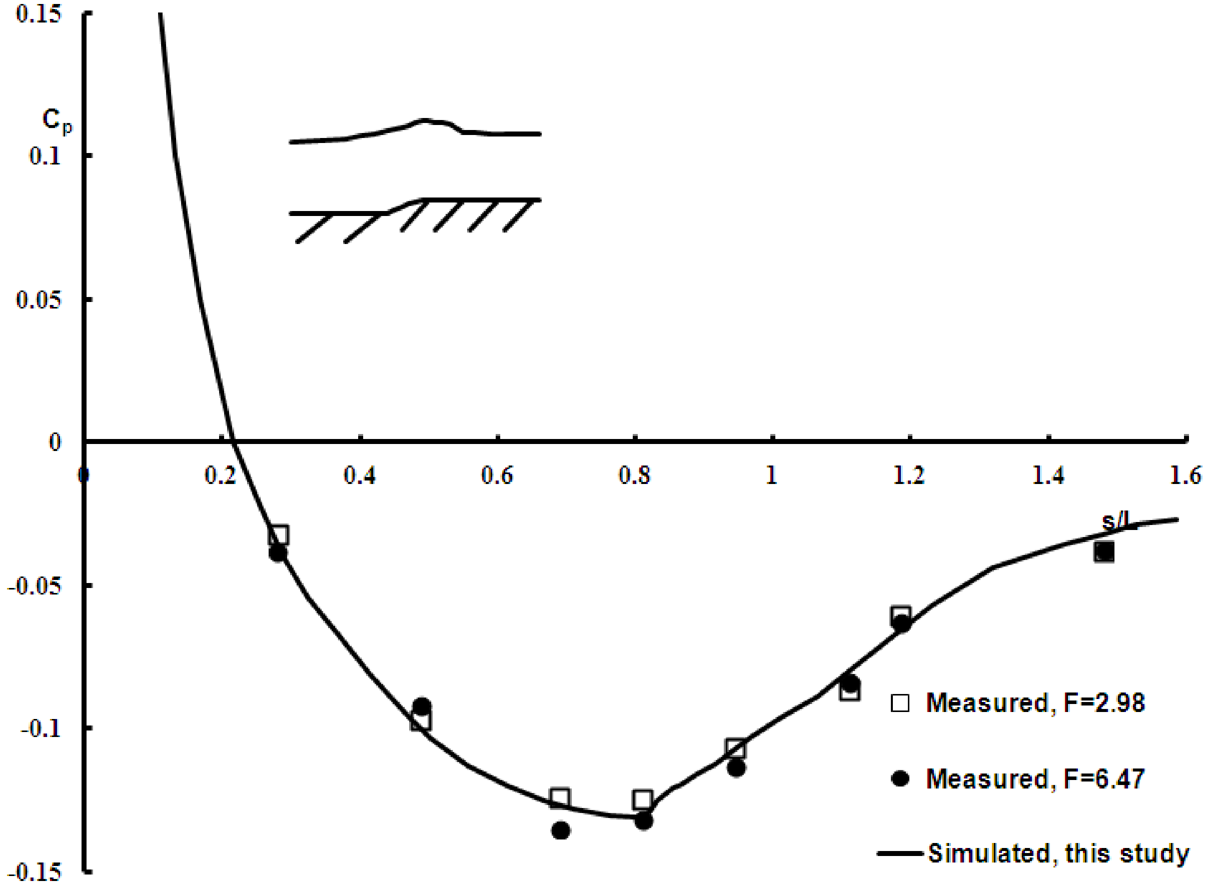

Figure 5. Comparison of the simulated (averaged, solid line) and measured (symbols) pressure coefficient distribution around the semi-arc step irregularity for F=2.98 and 6.47. Inset is the sketch of experimental set-up. *s* and *L* are the same as in Fig. 4.

(a)

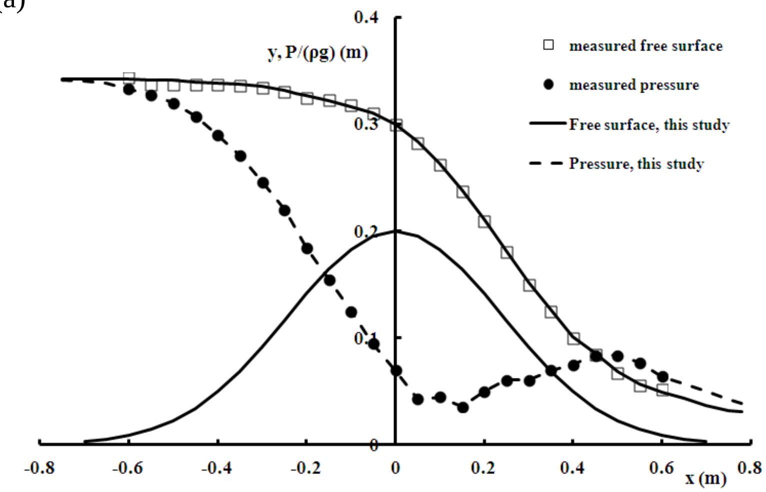

(b)

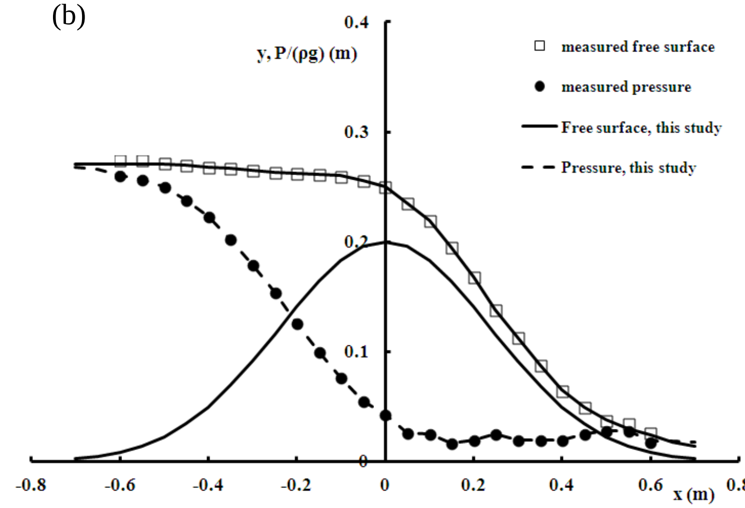

(c)

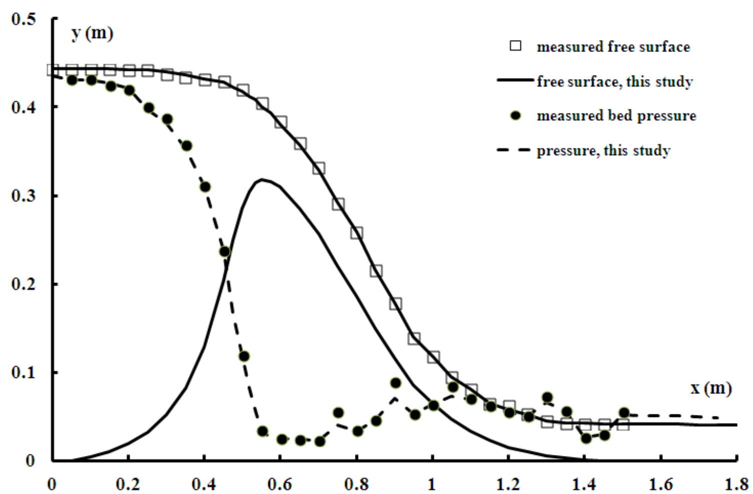

Figure 6. Plot of simulated (solid and dashed lines) and measured (symbols) free water surface and bottom pressure distribution of potential flow. (a) over a symmetrical hump for q=0.112 m^2/s and F= 0.18; (b) over a symmetrical hump for q=0.036 m^2/s and F= 0.08; and (c) over an asymmetrical hump for q=0.11165 m^2/s and F= 0.12.

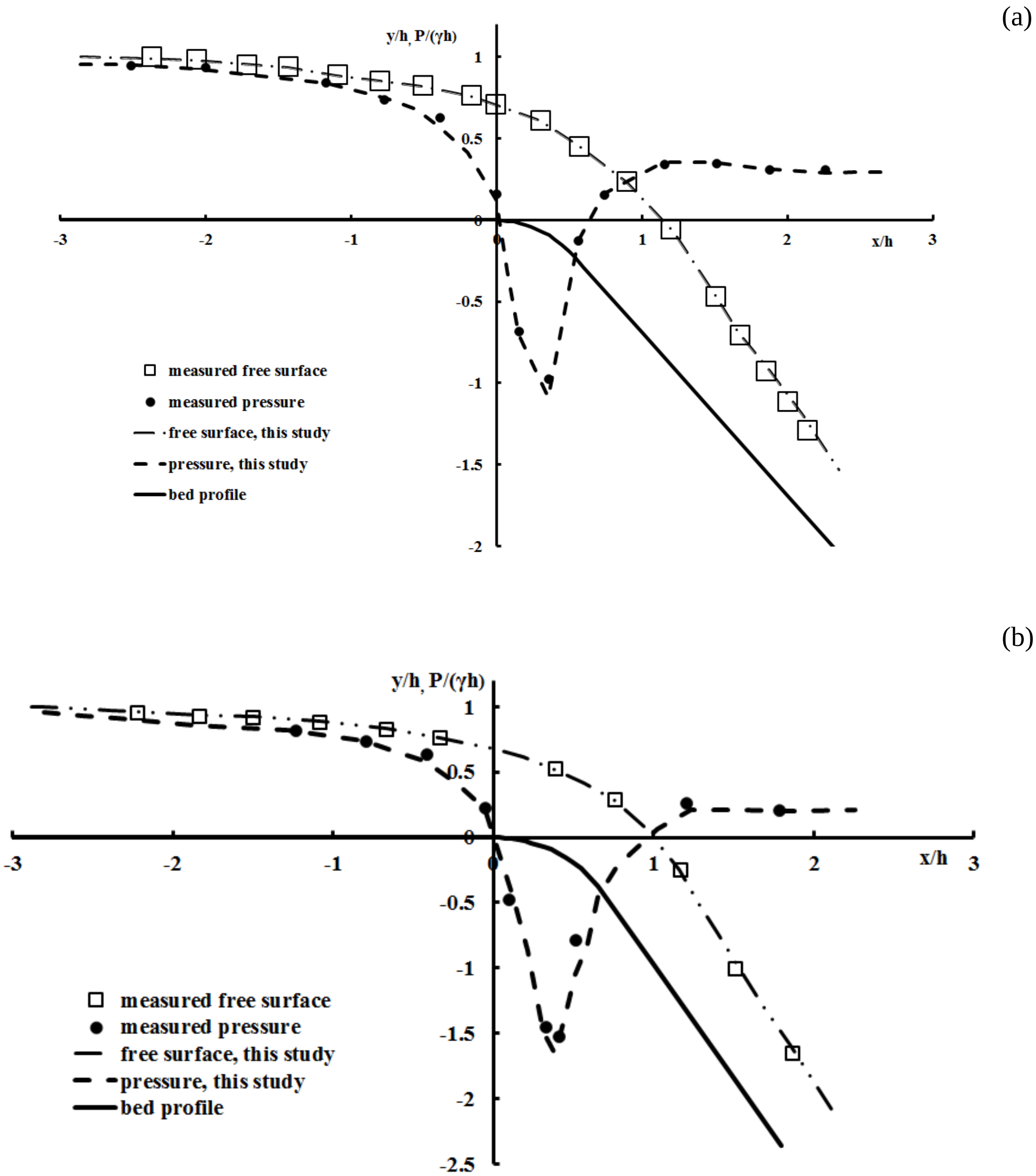

Figure 7 Simulated and measured free surface profile and bottom pressure distribution of the potential flow in transition from horizontal to steep slope for (a) steep slope = 45^0, F=1 and (b) steep slope = 60^0, F=1.

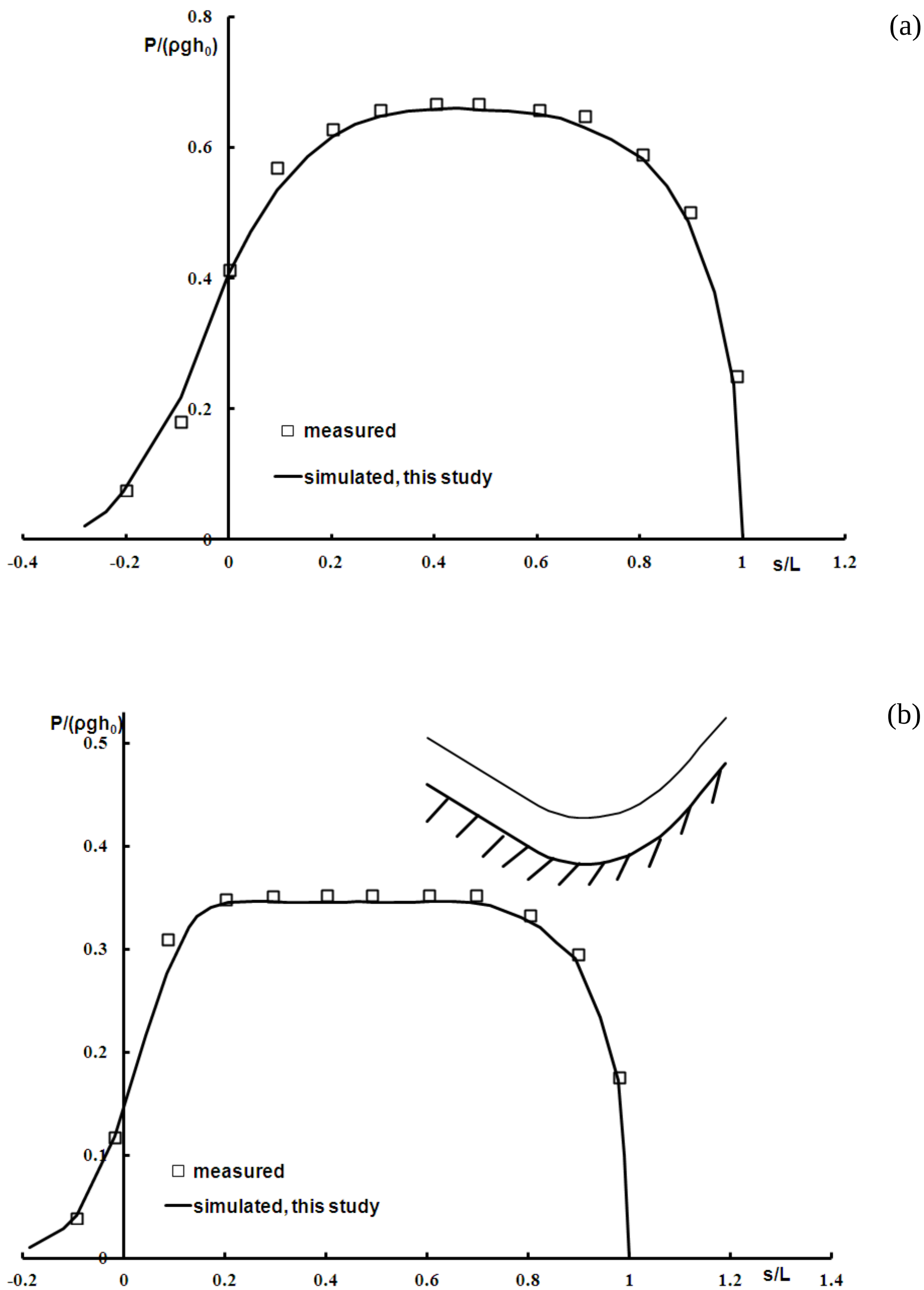

Figure 8 Comparison of simulated and measured flip bucket bottom pressure. The central angle of bucket is 95^0 and the slope angle of upstream spillway chute is 56.16^0 (inset is the sketch of experimental set-up). The incoming flow Froude number is (a) F=7.35; (b) F= 10.39.